ACTA ASTRONOMICA
Vol. **50** (2000) pp. 307–335

The Optical Gravitational Lensing Experiment. *BVI* Maps of Dense Stellar Regions. II. The Large Magellanic Cloud*

by

A. Udalski[1], M. Szymański[1], M. Kubiak[1],
G. Pietrzyński[1,2], I. Soszyński[1], P. Woźniak[3],
and K. Żebruń[1]

[1] Warsaw University Observatory, Al. Ujazdowskie 4, 00-478 Warszawa, Poland
e-mail: (udalski,msz,mk,pietrzyn,soszynsk,zebrun)@astrouw.edu.pl
[2] Universidad de Concepción, Departamento de Fisica, Casilla 160–C, Concepción, Chile
[3] Princeton University Observatory, Princeton, NJ 08544-1001, USA
e-mail: wozniak@astro.princeton.edu

Received September 18, 2000

ABSTRACT

We present the *BVI* photometric maps of the Large Magellanic Cloud. They contain *BVI* photometry and astrometry of more than 7 million stars from the central parts of the LMC. The data were collected during the second phase of the OGLE microlensing project. We discuss the accuracy of the data and present color-magnitude diagrams of all 26 fields observed by OGLE in the LMC.

The *BVI* maps of the LMC are accessible electronically for the astronomical community from the OGLE Internet archive.

Key words: *Magellanic Clouds – Surveys – Catalogs – Techniques: photometric*

1. Introduction

The Large Magellanic Cloud (LMC) is one of the most important astrophysical objects. This nearby galaxy hosts large variety of very important stellar populations and is an ideal laboratory for testing our understanding of stellar structure and evolution and for calibrating the most important standard candles. The LMC is also very important object for extragalactic astrophysics – the extragalactic distance scale is calibrated by the distance to the LMC. Due to relatively small distance from the Galaxy, stars and other objects from the LMC can easily be resolved and measured. Approximately the same distance to all objects from that galaxy makes

*Based on observations obtained with the 1.3 m Warsaw telescope at the Las Campanas Observatory of the Carnegie Institution of Washington.

it especially attractive for determination and comparison of basic parameters of different groups of stars.

Unfortunately, the LMC was relatively poorly observed, in particular with precise CCD techniques. Photometry of only selected fields in lines of sight usually toward star clusters in the halo of this galaxy can be found in literature. The situation considerably changed when the large microlensing surveys began regular monitoring of the Magellanic Clouds for microlensing events. The LMC is one of the most promising targets of the microlensing hunt, and therefore it was selected as a target of MACHO (Alcock *et al.* 2000) and EROS (Lasserre *et al.* 2000) microlensing projects. Large areas in the LMC were also observed by Zaritsky, Harris and Thompson (1997) as a part of a photometric survey of the Magellanic Clouds.

The LMC was included as one of the targets of the Optical Gravitational Lensing Experiment (OGLE) at the beginning of the second phase of the project (Udalski, Kubiak and Szymański 1997). Since January 1997 the large part of the central regions of the galaxy has been regularly observed practically on every clear night. As a result huge databases containing hundreds of photometric measurements of millions of stars were created.

The OGLE photometric data are particularly attractive for many projects requiring precise photometry. Among the other datasets collected during the microlensing searches, only the OGLE photometry was obtained with the standard *BVI* filters what makes it very well suited for projects not related to microlensing. Also, very good astronomical site where the OGLE project is conducted – the Las Campanas Observatory in Chile, made it possible to achieve the best resolution what is crucial in the very dense stellar fields of the LMC bar.

In this paper, which is the second of the series, we present "The OGLE *BVI* Maps of the LMC." The maps contain the mean *BVI* photometry and astrometry of more than 7 million stars from the field of about 5.7 square degrees in the central part of the LMC. With the maps of the Small Magellanic Cloud presented in the first paper of this series (Udalski *et al.* 1998b) they constitute a unique photometric database of objects from the Magellanic Clouds.

Because of potentially great impact on many astrophysical fields, the OGLE policy is to make the photometric data available to the astronomical community. Similarly to the SMC maps, the maps of the LMC are also available from the OGLE Internet archive. Details are provided in the last Section of this paper.

2. Observations

All observations presented in this paper were collected during the second phase of the OGLE microlensing search with the 1.3-m Warsaw telescope at the Las Campanas Observatory, Chile, which is operated by the Carnegie Institution of Washington. The telescope was equipped with the "first generation" camera with a SITe 2048×2048 CCD detector working in drift-scan mode. The pixel size was 24 μm giving the 0.417 arcsec/pixel scale. Observations were performed in the "slow" reading mode of the CCD detector with the gain 3.8 e^-/ADU and readout noise of about 5.4 e^-. Details of the instrumentation setup can be found in Udalski, Kubiak and Szymański (1997).

Table 1

Equatorial coordinates of the OGLE-II LMC fields

Field	RA (J2000)	DEC (J2000)
LMC_SC1	$5^h33^m49^s$	$-70°06'10''$
LMC_SC2	$5^h31^m17^s$	$-69°51'55''$
LMC_SC3	$5^h28^m48^s$	$-69°48'05''$
LMC_SC4	$5^h26^m18^s$	$-69°48'05''$
LMC_SC5	$5^h23^m48^s$	$-69°41'05''$
LMC_SC6	$5^h21^m18^s$	$-69°37'10''$
LMC_SC7	$5^h18^m48^s$	$-69°24'10''$
LMC_SC8	$5^h16^m18^s$	$-69°19'15''$
LMC_SC9	$5^h13^m48^s$	$-69°14'05''$
LMC_SC10	$5^h11^m16^s$	$-69°09'15''$
LMC_SC11	$5^h08^m41^s$	$-69°10'05''$
LMC_SC12	$5^h06^m16^s$	$-69°38'20''$
LMC_SC13	$5^h06^m14^s$	$-68°43'30''$
LMC_SC14	$5^h03^m49^s$	$-69°04'45''$
LMC_SC15	$5^h01^m17^s$	$-69°04'45''$
LMC_SC16	$5^h36^m18^s$	$-70°09'40''$
LMC_SC17	$5^h38^m48^s$	$-70°16'45''$
LMC_SC18	$5^h41^m18^s$	$-70°24'50''$
LMC_SC19	$5^h43^m48^s$	$-70°34'45''$
LMC_SC20	$5^h46^m18^s$	$-70°44'50''$
LMC_SC21	$5^h21^m14^s$	$-70°33'20''$
LMC_SC22	$5^h02^m26^s$	$-67°09'35''$
LMC_SC23	$5^h04^m45^s$	$-67°09'40''$
LMC_SC24	$5^h07^m05^s$	$-67°09'35''$
LMC_SC25	$5^h09^m24^s$	$-67°09'30''$
LMC_SC26	$5^h11^m43^s$	$-67°09'40''$

Observed fields covered practically the entire bar of the LMC. More than 4.5 square degrees (21 driftscan fields) were monitored regularly (practically on every clear night except for the May–August period each year) from January 1997 through May 2000. Five additional fields in the North–West part of the LMC were monitored on 13 nights between November 1998 and January 1999. Table 1 lists the equatorial coordinates of the centers of each field (14.2×57 arcmin) with their acronyms. Positions of the fields were chosen in that way that adjacent fields overlap by about one arcmin for testing purposes. Fig. 1 presents the picture of the LMC from the Digitized Sky Survey with contours of the OGLE-II fields.

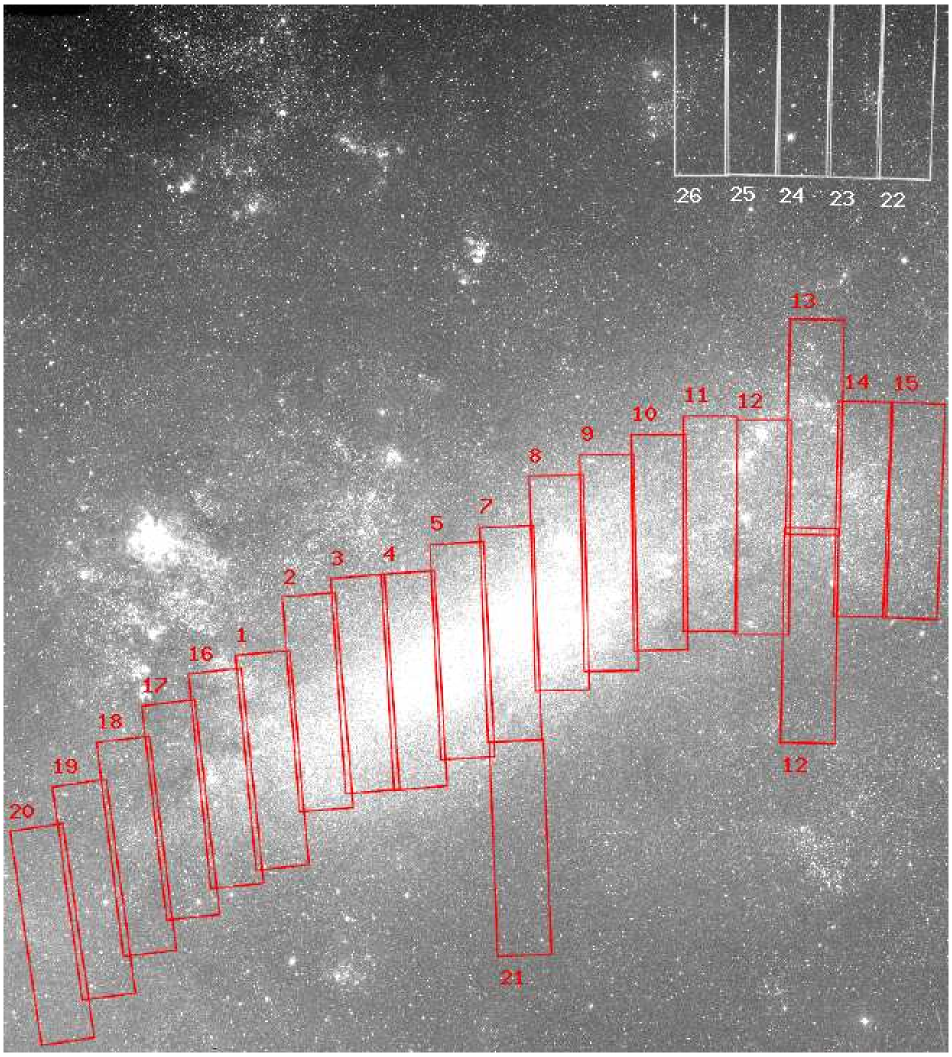

Fig. 1. OGLE-II fields in the LMC. North is up and East to the left in the Digitized Sky Survey image of the LMC.

Observations were obtained with the standard *BVI* filters closely reproducing the standard system (Section 3). Due to the microlensing search observing strategy, the vast majority of observations were obtained through the *I*-band filter (250–500 per field) while much smaller number of frames in the *BV*-bands were collected (25–40 and 40–80 for the *B* and *V* filters, respectively). For the additional North–West fields only 6 and 7 observations in the *V* and *I*-bands were collected. The effective exposure time was 125, 174 and 237 seconds, for the *I, V* and *B*-band, respectively.

Altogether more than 8800 images (about 300 GB of raw data) of the OGLE-II LMC fields were collected during the presented period of observations. Because of high stellar density of the bar fields, observations were only conducted during the nights with good seeing conditions. The median seeing of the entire data set is about 1.3 arcsec. Observations of the LMC were usually stopped when the seeing exceeded 1.6–1.8 arcsec.

3. Data Reduction and Calibration

All collected frames were reduced using the standard OGLE data pipeline in the identical manner as the SMC data (Udalski *et al.* 1998b). The data pipeline is described in detail in Udalski *et al.* (1998b). In short, after de-biasing and flat-fielding, photometry of objects is derived using the DOPHOT photometry program (Schechter, Saha and Mateo 1993) running in the fixed position mode on sixty four 512×512 pixel subframes. The full 2048×8192 pixel image being reduced is first matched with the so called "template" image, *i.e.*, the image with very good angular resolution (obtained at very good seeing conditions) and then divided into subframes. Photometry of each subframe is tied to the photometry of the template subframe by adding the mean shift derived usually from several hundreds brighter stars. Thus, photometry of the template image defines the instrumental system. Objects detected in the template images for the B and V-bands are first matched with the I-band template image objects of a given field so the star numbering is the same in all bands making the data handling much easier. Due to small shifts of the BV template images in respect to the I-band image not all stars detected in the I-band image have full BVI photometry. However, they usually have full photometry in the adjacent overlapping field.

To determine transformations of the instrumental photometry to the standard system, several Landolt (1992) standard fields were observed on about 250 photometric nights during the OGLE-II observations. Based on thousands of observations of standard stars in Landolt (1992) fields located all over the sky and covering large range of colors, the following average transformations were derived:

$$
\begin{aligned}
B &= b-0.034\times(B-V)+\mathrm{const}_B\\
V &= v-0.002\times(V-I)+\mathrm{const}_V\\
I &= i+0.029\times(V-I)+\mathrm{const}_I\\
B-V &= 0.963\times(b-v)+\mathrm{const}_{B-V}\\
V-I &= 0.969\times(v-i)+\mathrm{const}_{V-I}
\end{aligned}
\tag{1}
$$

The typical residuals of calculated minus observed magnitudes of standard stars did not exceed 0.03 mag. The transformations indicate that the OGLE-II filter system closely resembles the standard one, *i.e.*, the color coefficients are close to zero or one. Observations of standard stars also indicate that the instrumental system was extremely stable during the period of observations and the standard system magnitudes could be derived with good accuracy ($0.02-0.04$ mag) even during the photometric nights when no standard stars were observed.

Transformation of the instrumental magnitudes to the standard system consisted of the following steps. First, the aperture corrections were determined for each of the 64 subframes. They were determined from aperture photometry of typically 20–100 stars per subframe measured in the artificial images with faint stars subtracted. Then the total correction was determined consisting of the aperture correction, zero point of transformation, extinction correction and normalization to 1 sec exposure time. The total corrections were determined independently for about 10–25, 10–20 and 20–35 photometric nights for the *BV* and *I*-band, respectively. Typical standard deviation of the total correction in each of the 64 subframes was of about 0.015–0.020 mag. The averaged values of the total correction were subsequently used for the construction of photometric databases (Udalski *et al.* 1998b, Szymański and Udalski 1993) for the *B, V* and *I*-band. The databases contain entire photometry of all objects in a given OGLE field in the system very close to the standard one – only the color term (Eq. 1) is not included.

Equatorial coordinates of objects detected in the OGLE fields were determined in the identical manner as described in Udalski *et al.* (1998b). Objects in the OGLE-II frames were cross-identified with the objects detected in the Digitized Sky Survey images, and the transformation between the OGLE pixel grid and (RA,DEC) coordinates in the DSS coordinate system was determined. About 1700–7400 stars were used for transformation depending on the stellar density in the field. Internal accuracy of the determined equatorial coordinates, as measured in the overlapping regions of neighboring fields is about 0.15–0.20 arcsec. However, the systematic error of the DSS coordinate system may reach 0.7 arcsec.

4. *BVI* Maps of the LMC

The *BVI* maps of the LMC were constructed using the photometric databases of each field. First, the mean magnitudes of each object were calculated with 5σ rejection alghoritm. Then, we corrected the magnitudes for a small systematic error, caused by non-perfect flat-fielding at the edges of the field. This effect was first noticed by Dr. D.S. Graff (Ohio State University), and it was precisely mapped based on observations of hundreds of standard stars. Finally, the color corrections (Eq. 1) were derived and added. Only objects with more than 5, 10 and 40 good observations (see Udalski *et al.* 1998b) in the *BVI*-bands, respectively, were included in the final maps of the LMC (three in the *V* and *I*-band in the North–West LMC fields). Table 2 lists the total number of objects in the OGLE-II maps of the LMC fields.

Table 3 presents the sample data from the map of the LMC_SC3 field. In the consecutive columns the following data are provided: star ID number, equatorial coordinates, (X,Y) coordinates in the *I*-band template image, photometry: *V*, $(B-V)$, $(V-I)$, *B*, *I*, number of observations, number of rejected observations

Table 2

Number of objects in the OGLE-II LMC maps

Field	$N_{\rm objects}$	Field	$N_{\rm objects}$
LMC_SC1	348876	LMC_SC14	263522
LMC_SC2	421346	LMC_SC15	223214
LMC_SC3	448729	LMC_SC16	268601
LMC_SC4	485406	LMC_SC17	238924
LMC_SC5	460020	LMC_SC18	211320
LMC_SC6	474475	LMC_SC19	194556
LMC_SC7	477838	LMC_SC20	209089
LMC_SC8	368108	LMC_SC21	198156
LMC_SC9	397024	LMC_SC22	68061
LMC_SC10	292552	LMC_SC23	71475
LMC_SC11	352465	LMC_SC24	71012
LMC_SC12	215090	LMC_SC25	60276
LMC_SC13	272614	LMC_SC26	54083
		Total:	7146832

and standard deviation for the *BVI*-bands, respectively. In the electronic version we additionally provide the FITS template images for easy object identification. In the case of the North–West LMC fields only *V* and *I* images were collected. Therefore, the maps of these fields contain dummy values in the columns related to *B*-band photometry. Maps of all LMC fields are available electronically from the OGLE Internet archive (see Section 7).

5. Data Tests

5.1. Photometry

Quality of the OGLE-II photometry can be assessed from comparison of magnitudes of stars located in the overlaps between neighboring fields. Because each of the fields was calibrated independently such a comparison provides information on accuracy of calibration and the typical accuracy of photometry. Figs. 2, 3 and 4 present differences of magnitudes for stars with magnitudes brighter than $B = 20$ mag, $V = 20$ mag and $I = 19$ mag, plotted as a function of line number for three fields located in the central part of the LMC and at the West and East edges of the bar. For the remaining fields the plots look very similar. As can be seen the average difference of magnitudes is always below 0.01 mag indicating good consistency of the calibration procedure. The typical sigma of the Gaussian fitted to the histogram of differences of magnitudes is about 0.040, 0.035 and 0.025 mag for the *BVI*-bands, respectively.

Table 3

Sample of data from the *BVI* map of the field LMC_SC3

Star no	RA (J2000)	DEC (J2000)	X	Y	V	$B-V$	$V-I$	B	I	$N^B_{\rm ok}$	$N^B_{\rm bad}$	σ_B	$N^V_{\rm ok}$	$N^V_{\rm bad}$	σ_V	$N^I_{\rm ok}$	$N^I_{\rm bad}$	σ_I
1	$5^{\rm h}27^{\rm m}46\overset{\rm s}{.}52$	$-70^\circ15'47\overset{''}{.}6$	275.31	77.35	13.147	0.557	0.689	13.709	12.459	21	0	0.012	52	1	0.016	382	1	0.031
2	$5^{\rm h}28^{\rm m}03\overset{\rm s}{.}66$	$-70^\circ15'46\overset{''}{.}7$	485.35	80.59	16.241	2.948	2.596	19.208	13.643	12	0	0.522	56	0	0.307	382	0	0.138
3	$5^{\rm h}27^{\rm m}45\overset{\rm s}{.}67$	$-70^\circ16'01\overset{''}{.}5$	265.17	43.68	16.831	1.795	2.888	18.641	13.940	23	0	0.184	58	0	0.171	326	0	0.071
4	$5^{\rm h}28^{\rm m}03\overset{\rm s}{.}60$	$-70^\circ15'25\overset{''}{.}4$	484.35	131.92	16.762	1.713	2.338	18.488	14.423	23	0	0.084	56	0	0.063	406	2	0.025
5	$5^{\rm h}27^{\rm m}50\overset{\rm s}{.}65$	$-70^\circ15'08\overset{''}{.}9$	325.49	171.01	17.074	1.737	2.765	18.824	14.307	23	0	0.176	57	0	0.161	416	0	0.062
6	$5^{\rm h}27^{\rm m}29\overset{\rm s}{.}70$	$-70^\circ14'49\overset{''}{.}7$	68.34	215.98	16.934	4.410	2.856	21.368	14.076	11	0	0.314	50	0	0.215	394	0	0.170
7	$5^{\rm h}27^{\rm m}24\overset{\rm s}{.}73$	$-70^\circ14'29\overset{''}{.}1$	7.13	265.23	18.086	–	3.786	–	14.296	0	0	–	29	0	0.265	318	0	0.140
8	$5^{\rm h}27^{\rm m}38\overset{\rm s}{.}43$	$-70^\circ13'28\overset{''}{.}2$	174.30	413.48	14.972	0.677	0.769	15.653	14.202	18	1	0.020	58	0	0.012	416	0	0.013
9	$5^{\rm h}27^{\rm m}56\overset{\rm s}{.}02$	$-70^\circ13'20\overset{''}{.}0$	390.14	434.47	16.565	1.847	2.326	18.425	14.236	23	0	0.054	58	0	0.034	419	0	0.018
10	$5^{\rm h}27^{\rm m}35\overset{\rm s}{.}32$	$-70^\circ13'17\overset{''}{.}6$	136.03	439.01	17.185	1.894	2.917	19.093	14.264	23	0	0.197	58	0	0.234	402	0	0.121
11	$5^{\rm h}28^{\rm m}03\overset{\rm s}{.}09$	$-70^\circ13'08\overset{''}{.}4$	476.77	463.04	15.957	1.745	2.331	17.715	13.624	23	0	0.080	58	0	0.050	402	0	0.026
12	$5^{\rm h}27^{\rm m}51\overset{\rm s}{.}54$	$-70^\circ13'00\overset{''}{.}1$	334.94	482.34	17.646	1.901	3.470	19.562	14.173	23	0	0.134	57	0	0.147	408	0	0.075
14	$5^{\rm h}27^{\rm m}39\overset{\rm s}{.}92$	$-70^\circ16'10\overset{''}{.}2$	194.78	22.33	16.419	1.705	1.749	18.134	14.668	6	1	0.012	57	0	0.023	263	0	0.018
15	$5^{\rm h}27^{\rm m}43\overset{\rm s}{.}91$	$-70^\circ16'05\overset{''}{.}6$	243.67	33.66	16.683	1.737	1.742	18.432	14.940	23	0	0.037	57	0	0.031	292	0	0.027
16	$5^{\rm h}27^{\rm m}40\overset{\rm s}{.}01$	$-70^\circ15'53\overset{''}{.}4$	195.66	62.91	15.218	0.662	0.771	15.884	14.446	18	0	0.013	54	0	0.016	389	2	0.017
17	$5^{\rm h}27^{\rm m}34\overset{\rm s}{.}48$	$-70^\circ15'43\overset{''}{.}2$	127.80	87.10	15.966	1.357	1.297	17.332	14.668	22	0	0.027	54	1	0.010	401	2	0.014
18	$5^{\rm h}27^{\rm m}25\overset{\rm s}{.}02$	$-70^\circ15'33\overset{''}{.}0$	11.66	111.04	16.766	–	1.641	–	15.123	0	0	–	40	0	0.020	336	3	0.016
19	$5^{\rm h}27^{\rm m}38\overset{\rm s}{.}54$	$-70^\circ15'23\overset{''}{.}5$	177.21	134.87	16.792	1.626	1.578	18.429	15.212	23	0	0.045	56	0	0.011	414	2	0.012
20	$5^{\rm h}27^{\rm m}51\overset{\rm s}{.}46$	$-70^\circ15'16\overset{''}{.}8$	335.48	152.15	16.870	1.720	2.022	18.602	14.847	23	0	0.057	58	0	0.027	413	3	0.016
21	$5^{\rm h}27^{\rm m}50\overset{\rm s}{.}36$	$-70^\circ15'12\overset{''}{.}1$	322.02	163.25	16.762	1.751	1.800	18.524	14.960	23	0	0.063	58	0	0.025	406	0	0.018
22	$5^{\rm h}27^{\rm m}24\overset{\rm s}{.}41$	$-70^\circ15'08\overset{''}{.}8$	3.80	169.41	16.446	–	1.663	–	14.783	0	0	–	33	1	0.030	274	0	0.021

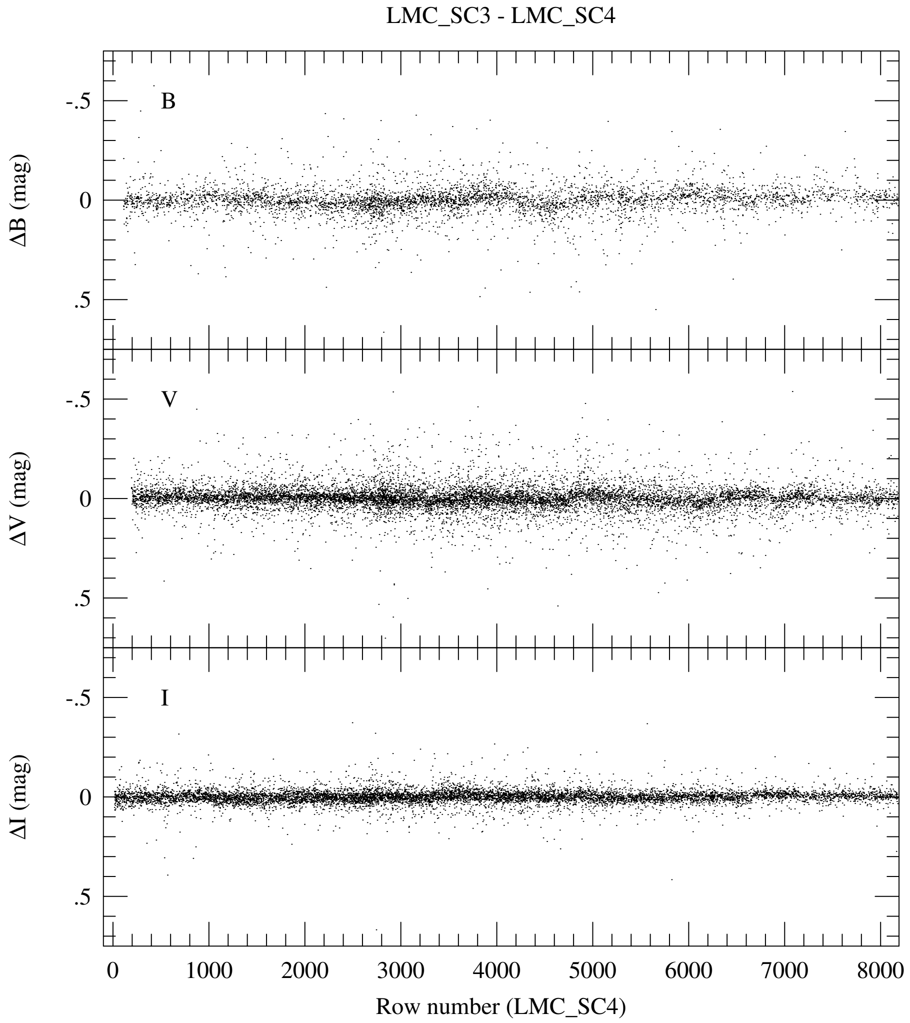

Fig. 2. Differences of magnitudes of the same objects in the overlapping regions of fields LMC_SC3 and LMC_SC4.

The error of photometric measurements is a function of stellar magnitude. To illustrate that dependence Figs. 5 and 6 show the standard deviation of *B, V* and *I*-band magnitudes of objects in the central field LMC_SC6 and much less crowded LMC_SC12. Only about 50 000 stars are plotted for clarity.

Accuracy of the zero points of the OGLE photometry can be estimated from comparison of the OGLE data with other observations. Unfortunately, the number of good quality photometric data from the LMC bar is very limited. These regions were rarely observed in the past, in particular with precise CCD detectors. We have found in the literature only three cases we can compare our data with.

Udalski *et al.* (1998a) presented comparison of the *I*-band light curves of Ce-

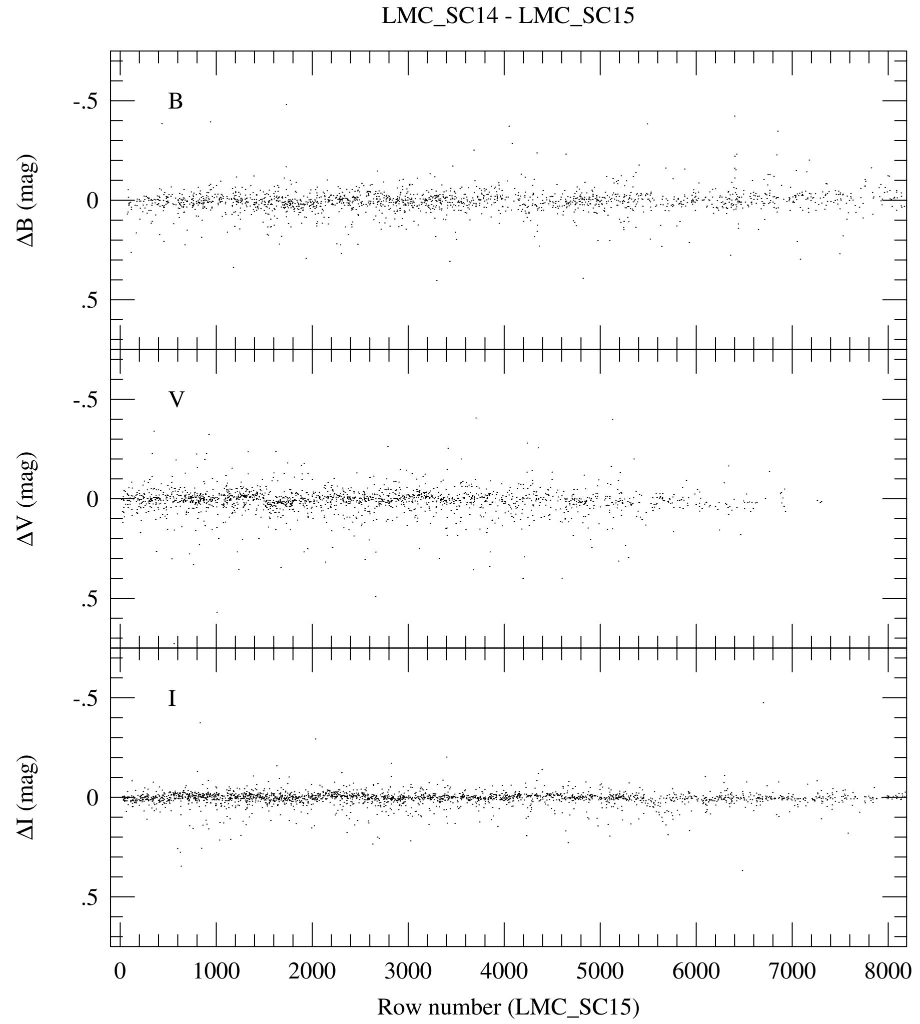

Fig. 3. Differences of magnitudes of the same objects in the overlapping regions of fields LMC_SC14 and LMC_SC15.

pheids located close to NGC 1850 with those obtained by Sebo and Wood (1995) indicating good agreement of the zero points of both data sets. Although the LMC data were only preliminarily calibrated at that time, the final calibration of that OGLE field is different only by a few thousandths of magnitude. Therefore the conclusion of Udalski *et al.* (1998a) fully holds.

Walker (1993) presented *BV* photometry of stars in the field of NGC 1835. In addition to the photometry of variable stars he also published magnitudes of nine local standard stars. One of these stars (#11) turned out to be a small amplitude long term variable as indicated by the OGLE data. One of the remaining eight stars (#4) is brighter by about 0.25 mag than indicated by the OGLE photometry. Al-

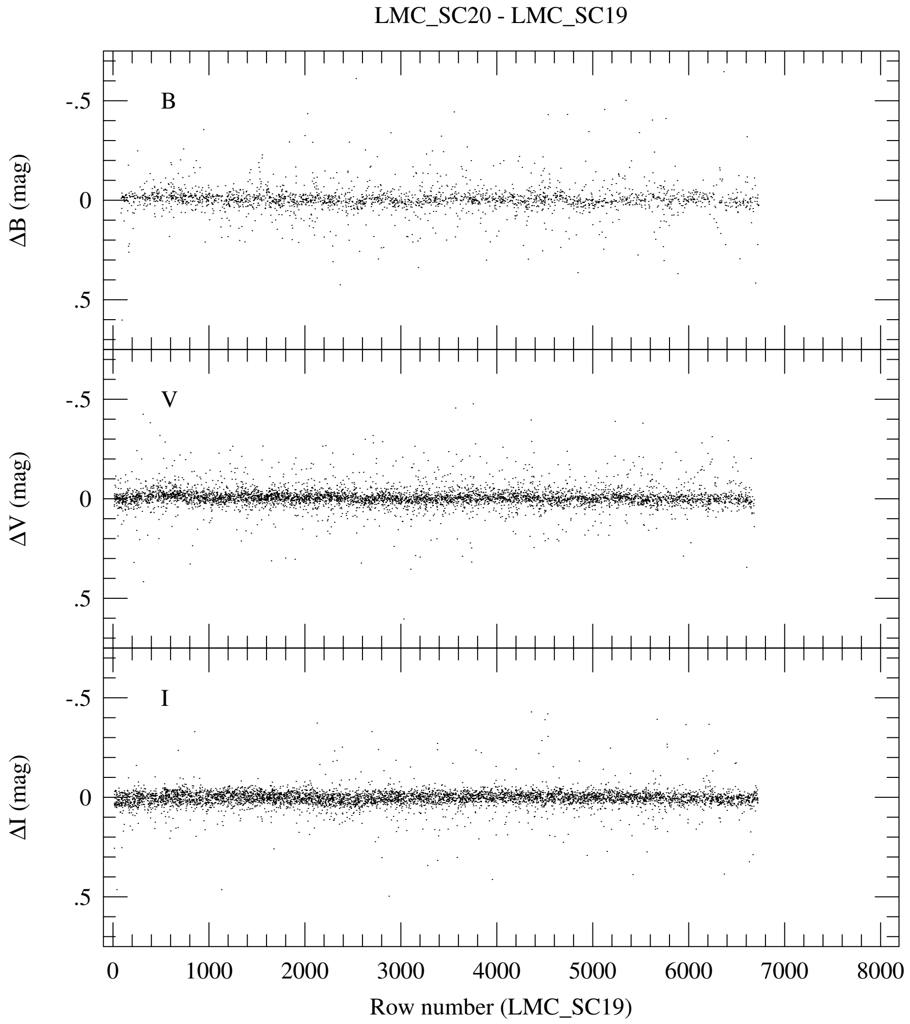

Fig. 4. Differences of magnitudes of the same objects in the overlapping regions of fields LMC_SC20 and LMC_SC19.

though the OGLE data do not show any larger light variations of this object, it is likely that so large discrepancy might be caused by some long term activity. Also OGLE data indicate that the star #6 is significantly fainter (more than 0.1 mag) than according to Walker. For the remaining six objects the mean difference of V magnitudes is equal to: $\Delta V = -0.026 \pm 0.025$ mag indicating good agreement of both data sets. Walker's magnitudes are slightly brighter. Comparison of $B-V$ colors of Walker standards with the OGLE data indicates, however, that for stars redder than $(B-V) \approx 1.2$ mag the OGLE colors are by more than 0.1 mag redder. For the four Walker standards outside that range the agreement is good – the mean difference of $(B-V)$ is equal to $\Delta(B-V) = -0.026 \pm 0.028$ mag with Walker's colors

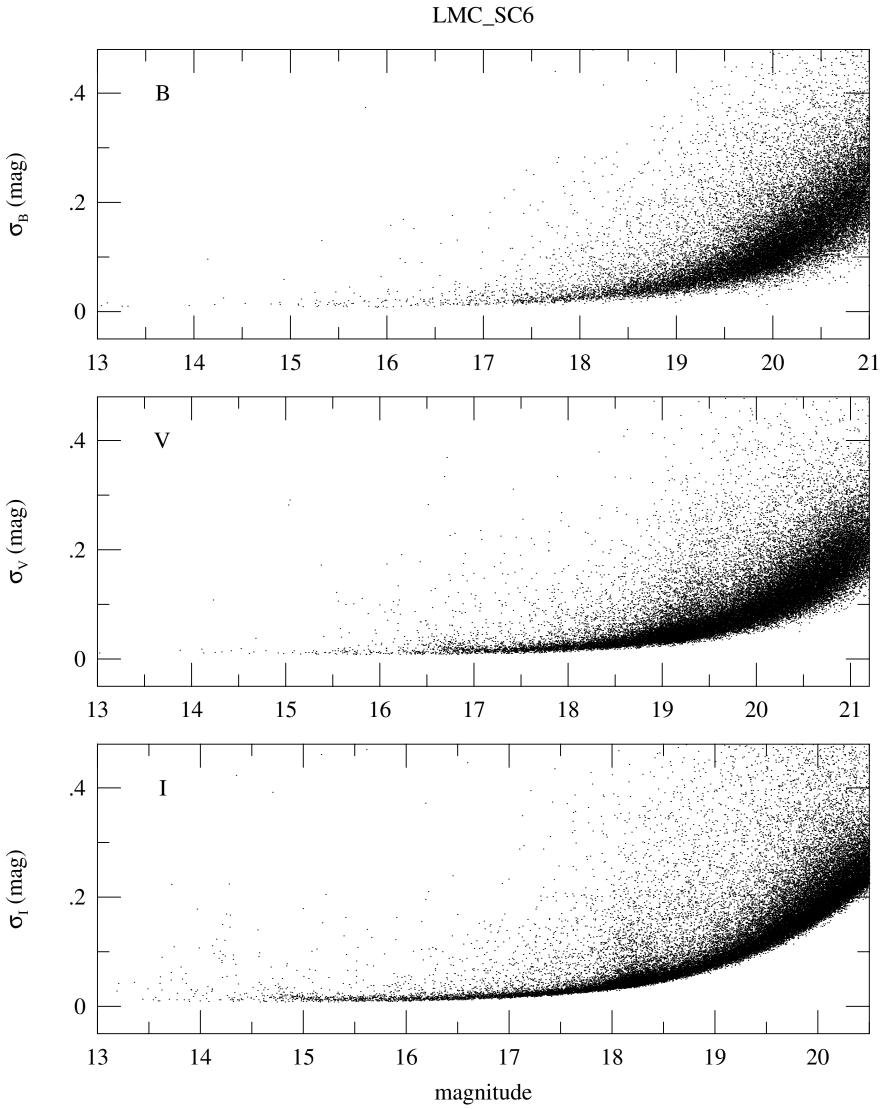

Fig. 5. Standard deviation of magnitudes of objects in the field LMC_SC6.

being bluer. The discrepancy for redder stars is somewhat worrying. However, the Walker *B*-band filter rather poorly matched the standard *B*-band (color coefficient of transformation of about 1.2; see Walker 1992) and therefore larger systematic color differences for stars with extreme red colors are very likely. Apart from this problem the overall agreement between the Walker's and OGLE *BV* photometry calibrations is quite good.

Finally, Clementini *et al.* (2000) presented photometry of two fields located close to the LMC bar. One of their fields, Field A, overlaps in large part with the OGLE field LMC_SC21. Unfortunately, a couple of local standard stars for which

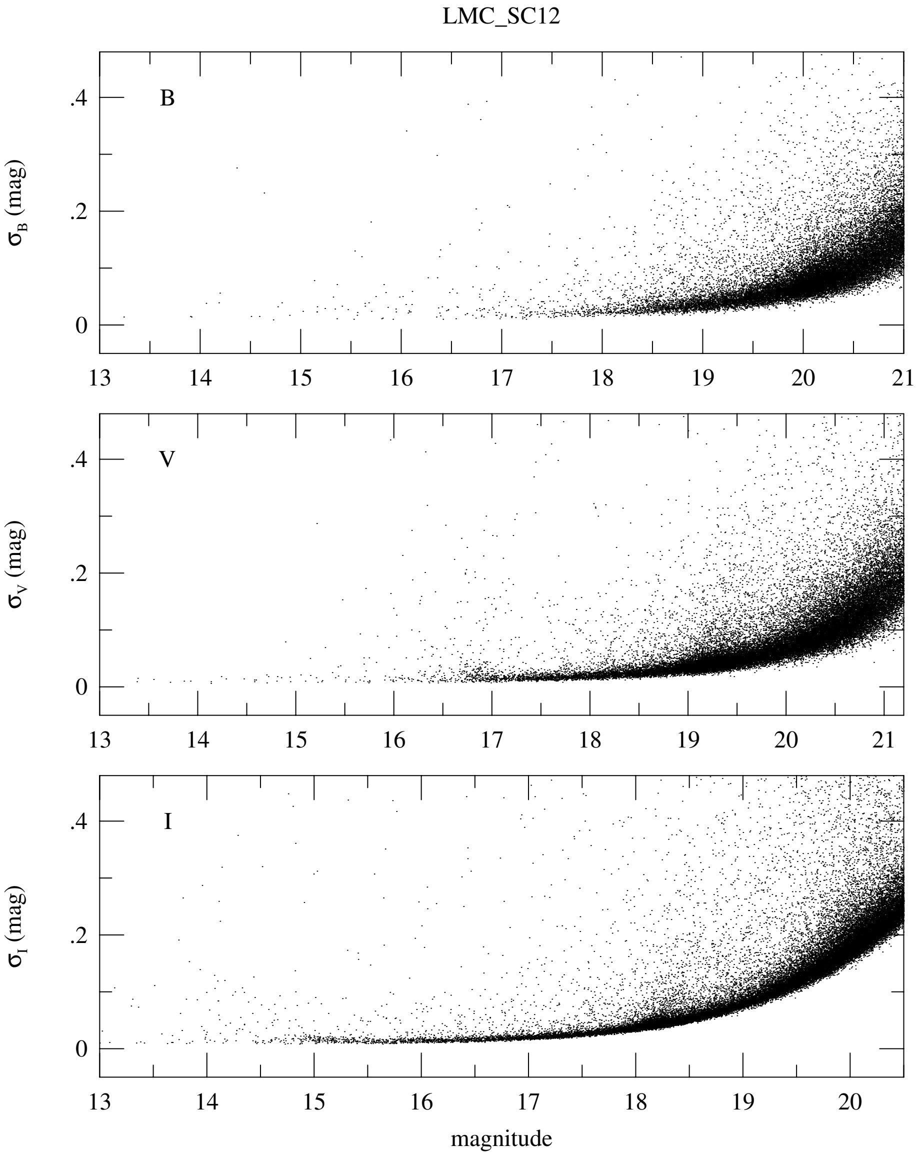

Fig. 6. Standard deviation of magnitudes of objects in the field LMC_SC12.

BV photometry is presented by Clementini *et al.* (2000) are located outside the OGLE field. Therefore the only comparison with the OGLE photometry which can be made is based on the average magnitudes of groups of stars, namely RR Lyr and red clump stars.

We extracted RR Lyr and red clump stars located in the LMC_SC21 field and limited these samples to objects with declination within the Clementini *et al.* (2000) Field A limits. One should be aware that the two compared regions are not exactly the same, but because the interstellar extinction is quite uniform in this part of the

LMC it is very unlikely to introduce any significant error by limiting the OGLE field in declination only. On the other hand much larger sample of stars can be averaged (in particular RR Lyr stars) making the mean magnitudes much more reliable.

For RR Lyr stars (71 objects) the intensity mean magnitudes were first derived. Then the average magnitudes of both RR Lyr and red clump stars were calculated. Comparison with Clementini *et al.* (2000) values yields: RR Lyr – $\langle V\rangle = 19.35$ mag *vs.* $\langle V\rangle = 19.37$ mag and $\langle B-V\rangle = 0.41$ mag *vs.* $\langle B-V\rangle = 0.37$ mag, for Clementini *et al.* (2000) and OGLE, respectively. For red clump stars – $\langle V\rangle = 19.22$ mag *vs.* $\langle V\rangle = 19.24$ mag and $\langle B-V\rangle = 0.92$ mag *vs.* $\langle B-V\rangle = 0.93$ mag, again for Clementini *et al.* (2000) and OGLE, respectively. As can be seen the agreement between those two photometric data sets is also very good. Comparison of red clump stars is certainly much more sound because of two orders of magnitude larger number of stars.

Summarizing, comparison of the OGLE *BVI* photometry with other observations indicates that in each band the agreement of the zero points is quite good. Because the OGLE calibrations were obtained on large number of photometric nights with use of wide range of standard fields they are certainly very reliable. We estimate the uncertainty of the zero points to be less than 0.02 mag. The OGLE-II maps constitute a huge set of secondary standards in the LMC line of sight.

5.2. *Completeness*

To estimate the completeness of detection of stars in the OGLE fields we performed similar set of tests as in the case of the SMC maps. For details the reader is referred to Udalski *et al.* (1998b). Table 4 presents results of these tests for three fields of different stellar density. As can be seen the completeness is high down to stars as faint as $I \approx 19.5$ mag, $V \approx 20$ mag and $B \approx 20$ mag. For fainter stars it gradually drops. The completeness is also a function of stellar density of the field.

6. Color-Magnitude Diagrams

Figs. 7–19 show I *vs.* $(V-I)$ color-magnitude diagrams (CMDs) of all LMC fields. They are presented to illustrate quality of data and potential usefulness of the OGLE LMC maps for studying many important astrophysical problems. About 25000 stars (*i.e.*, about 5–50% of the total number) from each field are plotted in these figures for clarity.

The CMDs presented in Figs. 7–19 reveal in great detail the most characteristic features of the LMC population of stars: main sequence stars, red giant branch stars, prominent red clump etc. The shape of the red clump can be an indicator of regions with non-uniform extinction in the LMC. For instance, red clump is severely elongated in the direction of reddening in the fields LMC_SC16–18, while relatively round in the center of the bar (fields LMC_SC2–6).

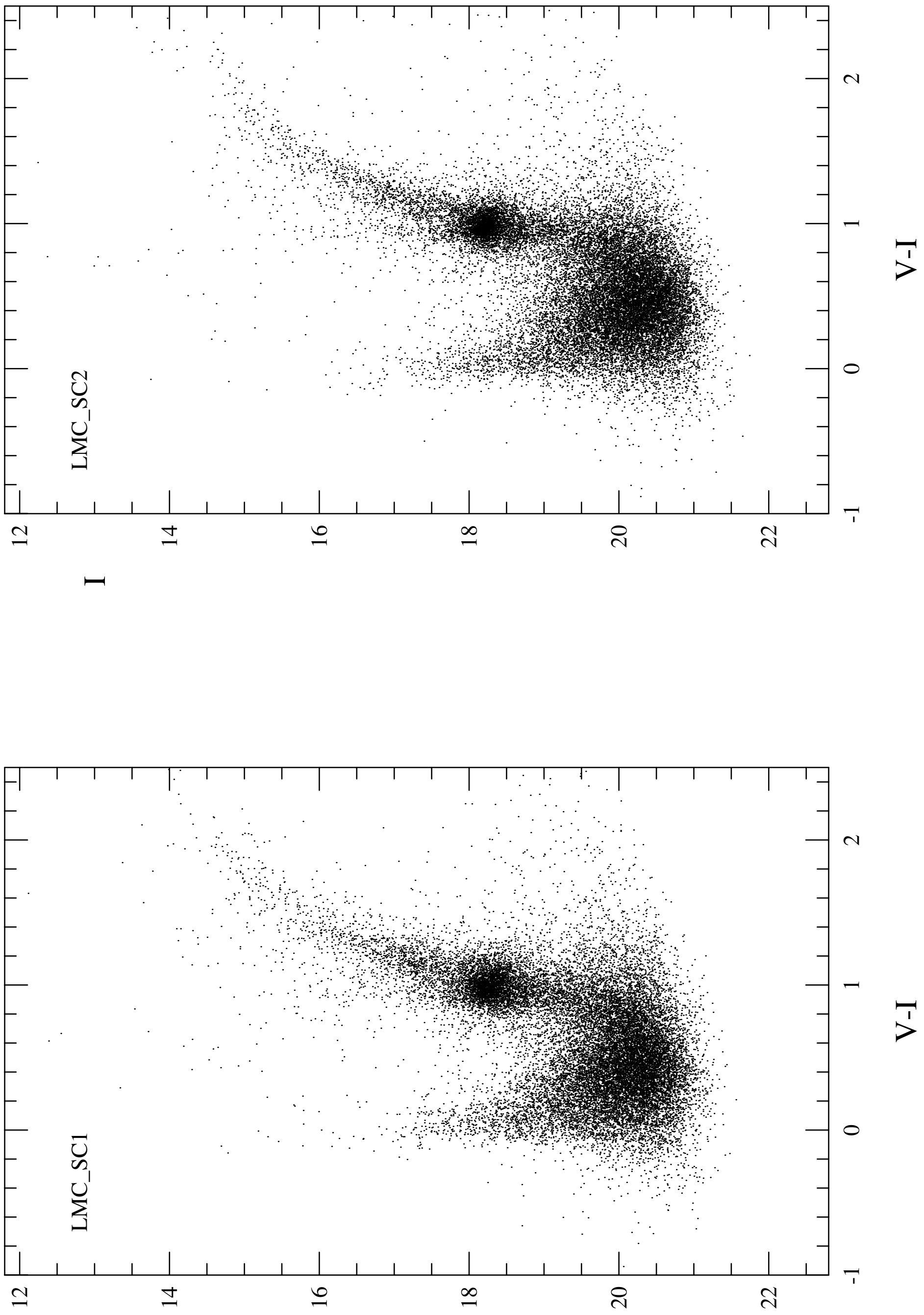

Fig. 7. Color-magnitude diagrams of the fields LMC_SC1 and LMC_SC2.

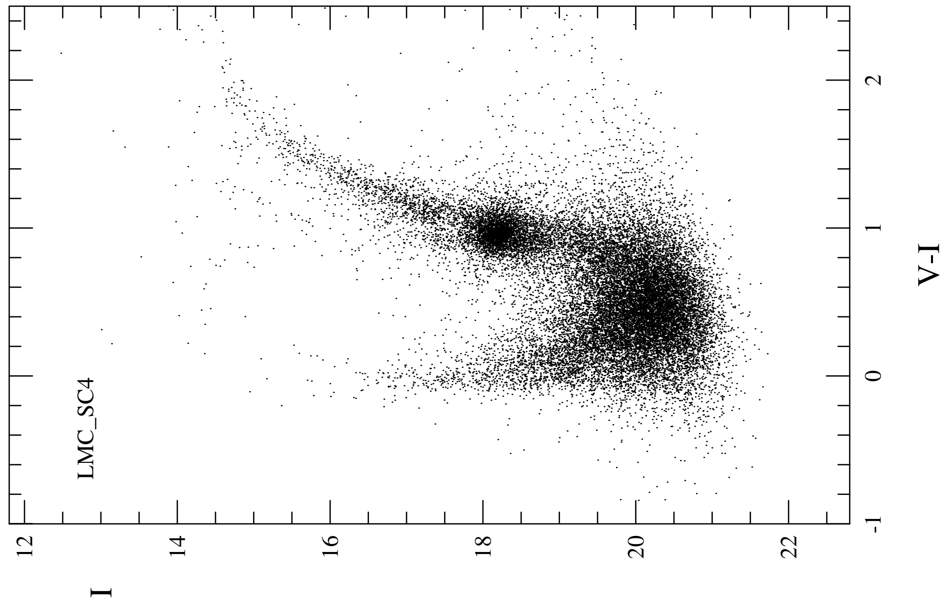

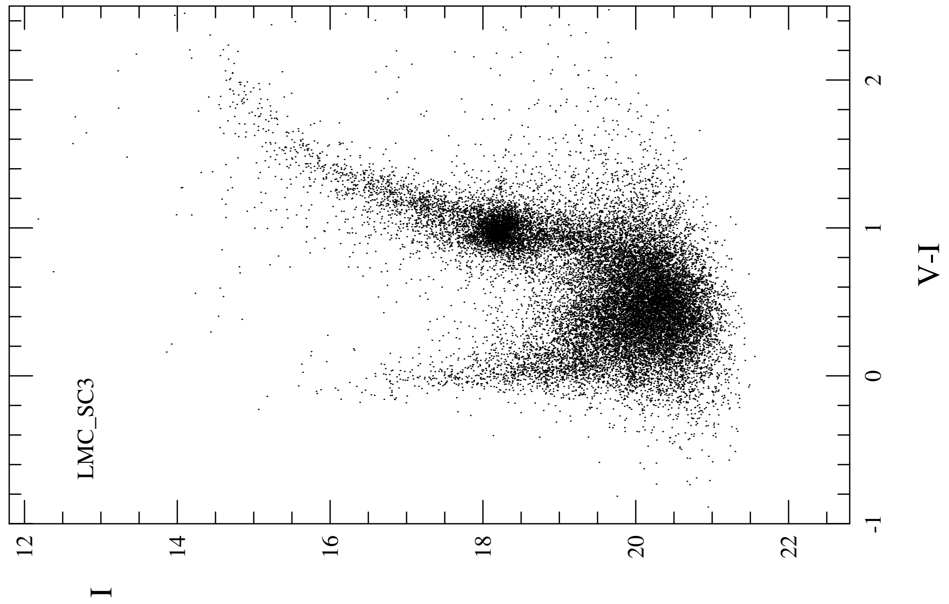

Fig. 8. Color-magnitude diagrams of the fields LMC_SC3 and LMC_SC4.

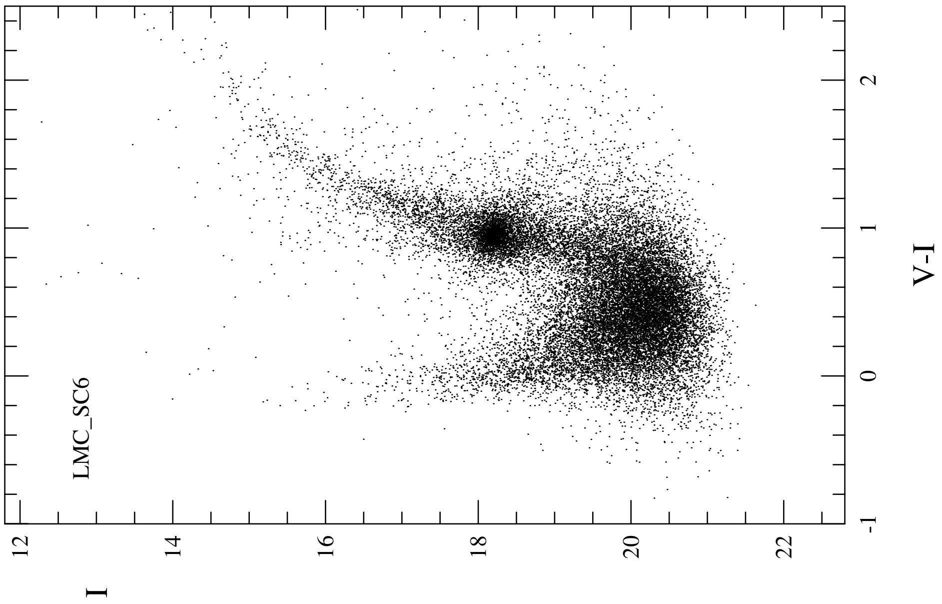

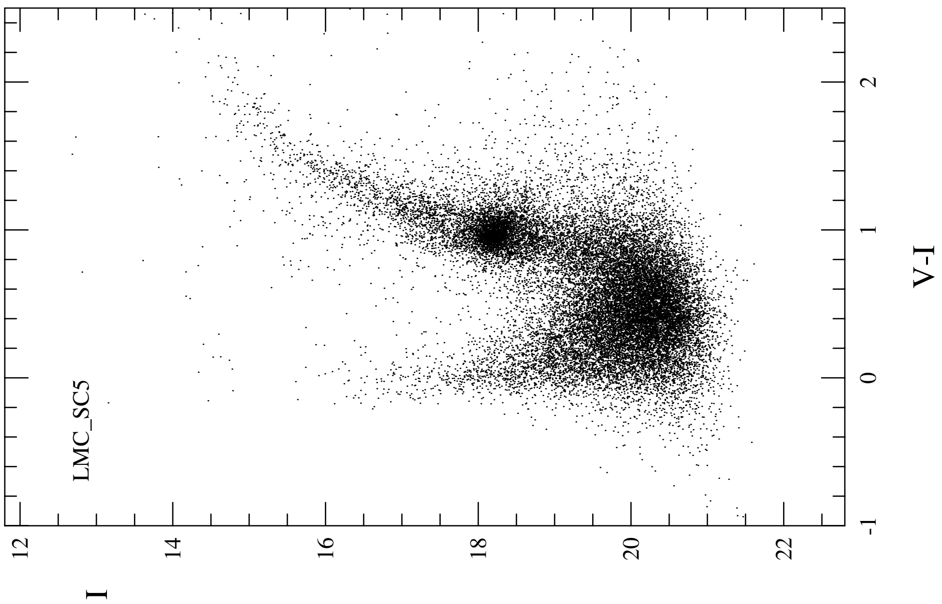

Fig. 9. Color-magnitude diagrams of the fields LMC_SC5 and LMC_SC6.

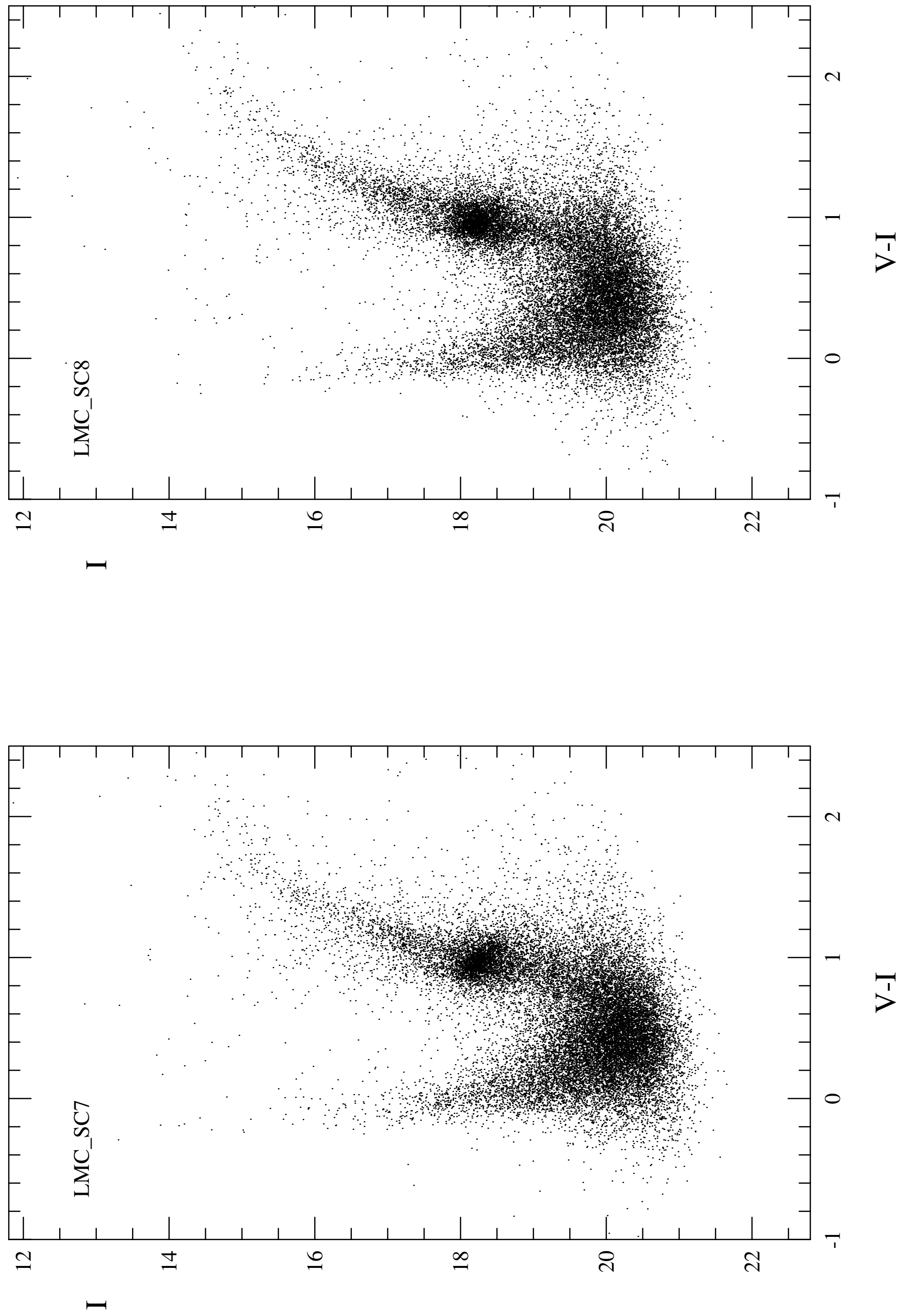

Fig. 10. Color-magnitude diagrams of the fields LMC_SC7 and LMC_SC8.

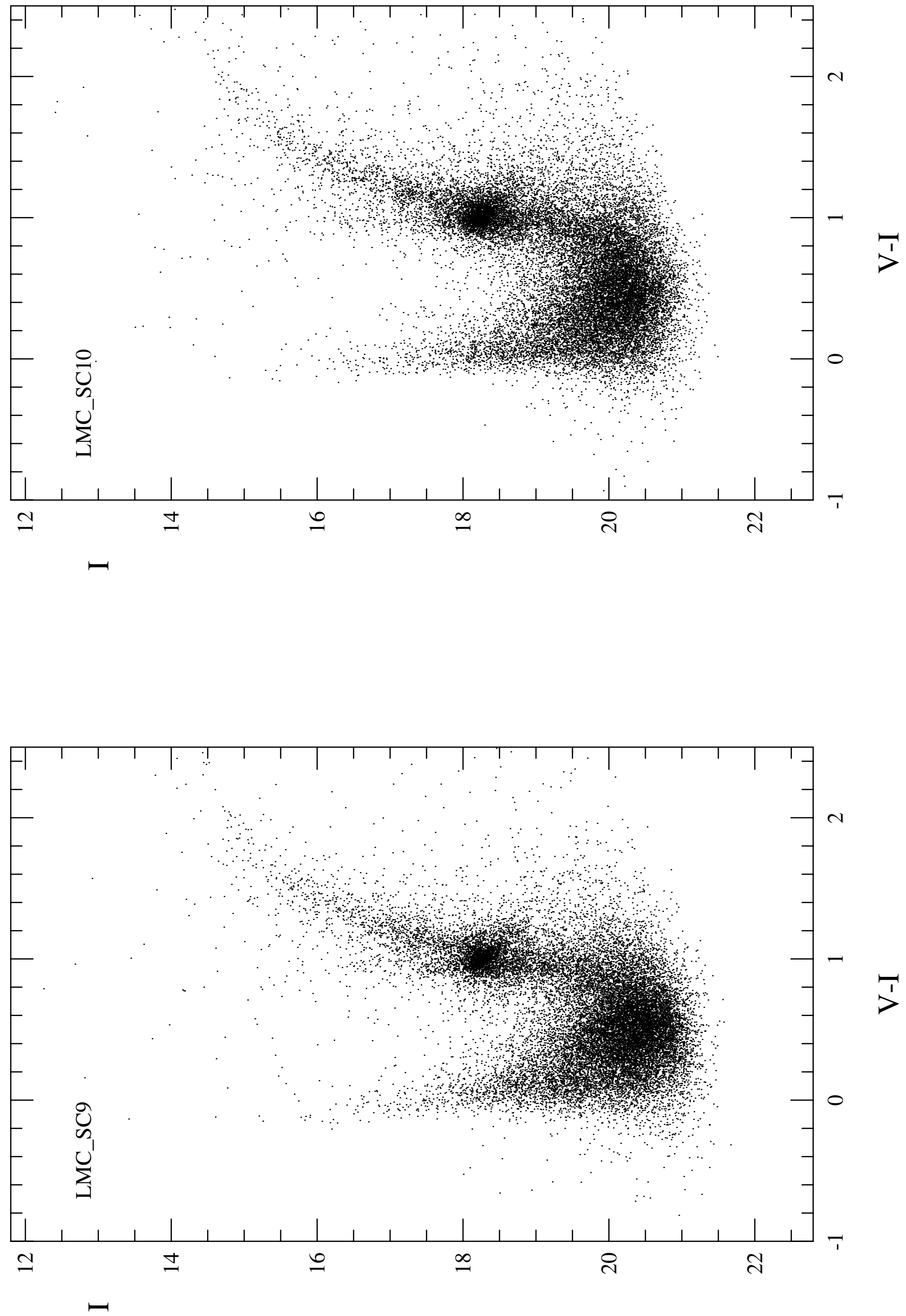

Fig. 11. Color-magnitude diagrams of the fields LMC_SC9 and LMC_SC10.

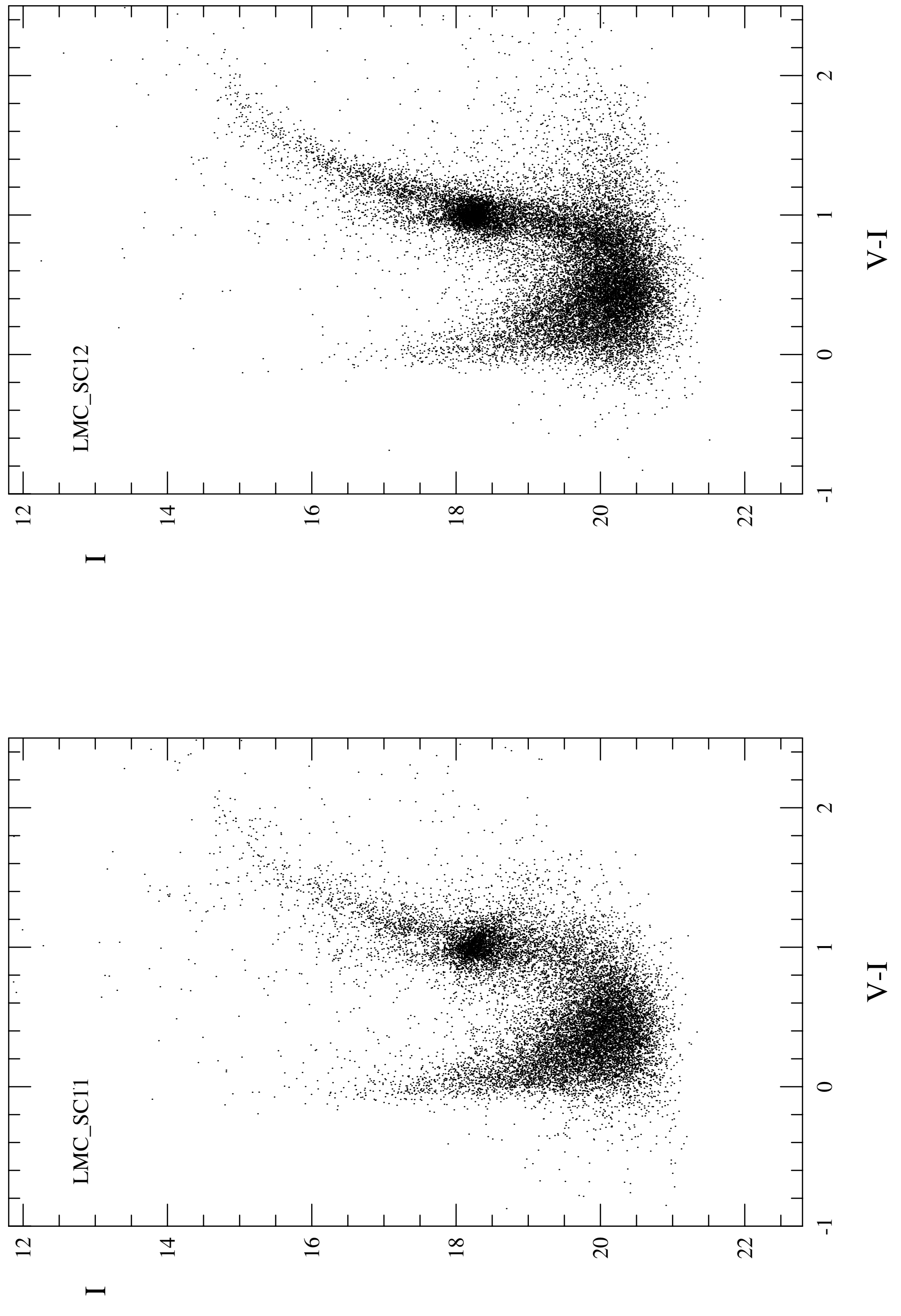

Fig. 12. Color-magnitude diagrams of the fields LMC_SC11 and LMC_SC12.

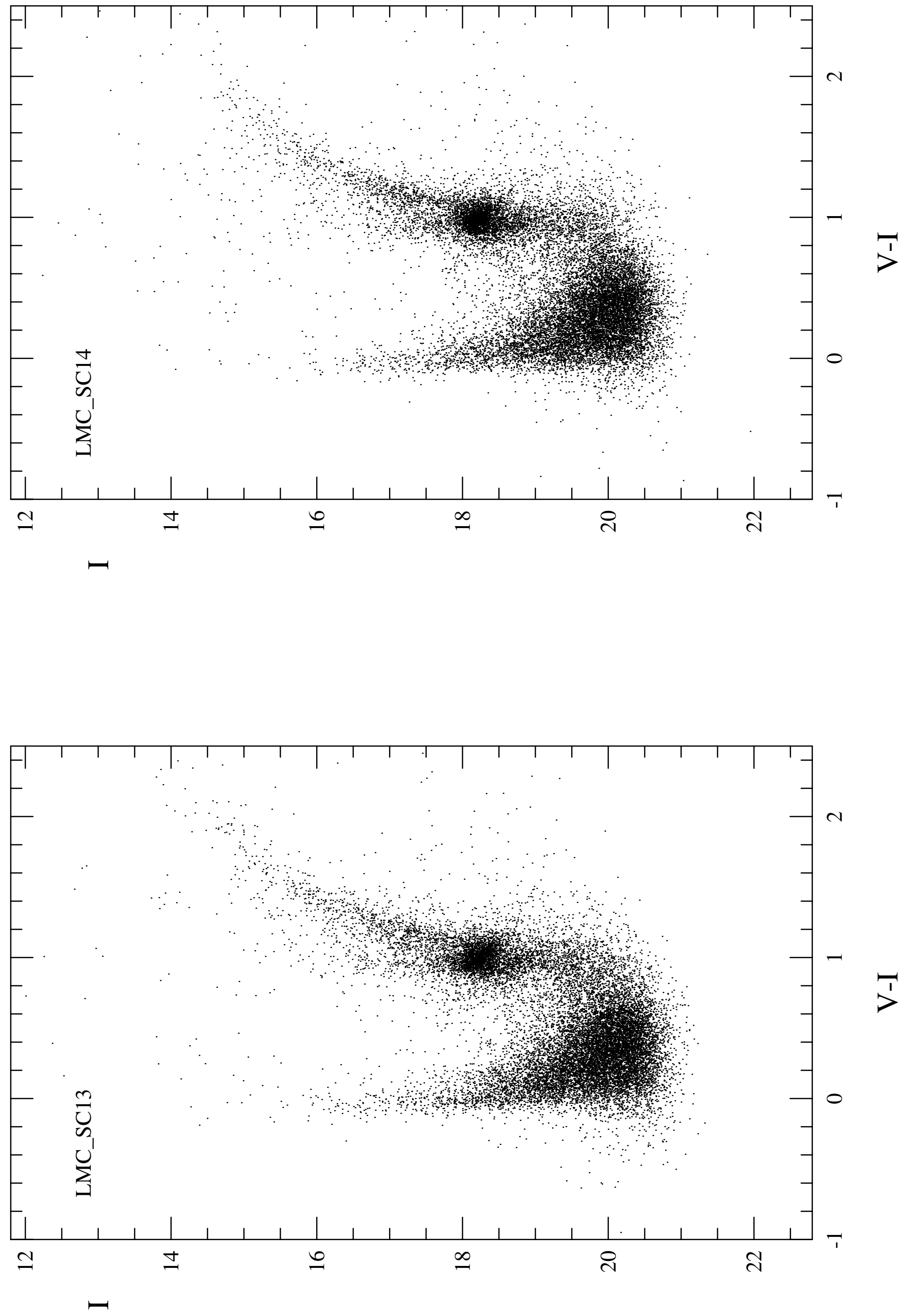

Fig. 13. Color-magnitude diagrams of the fields LMC_SC13 and LMC_SC14.

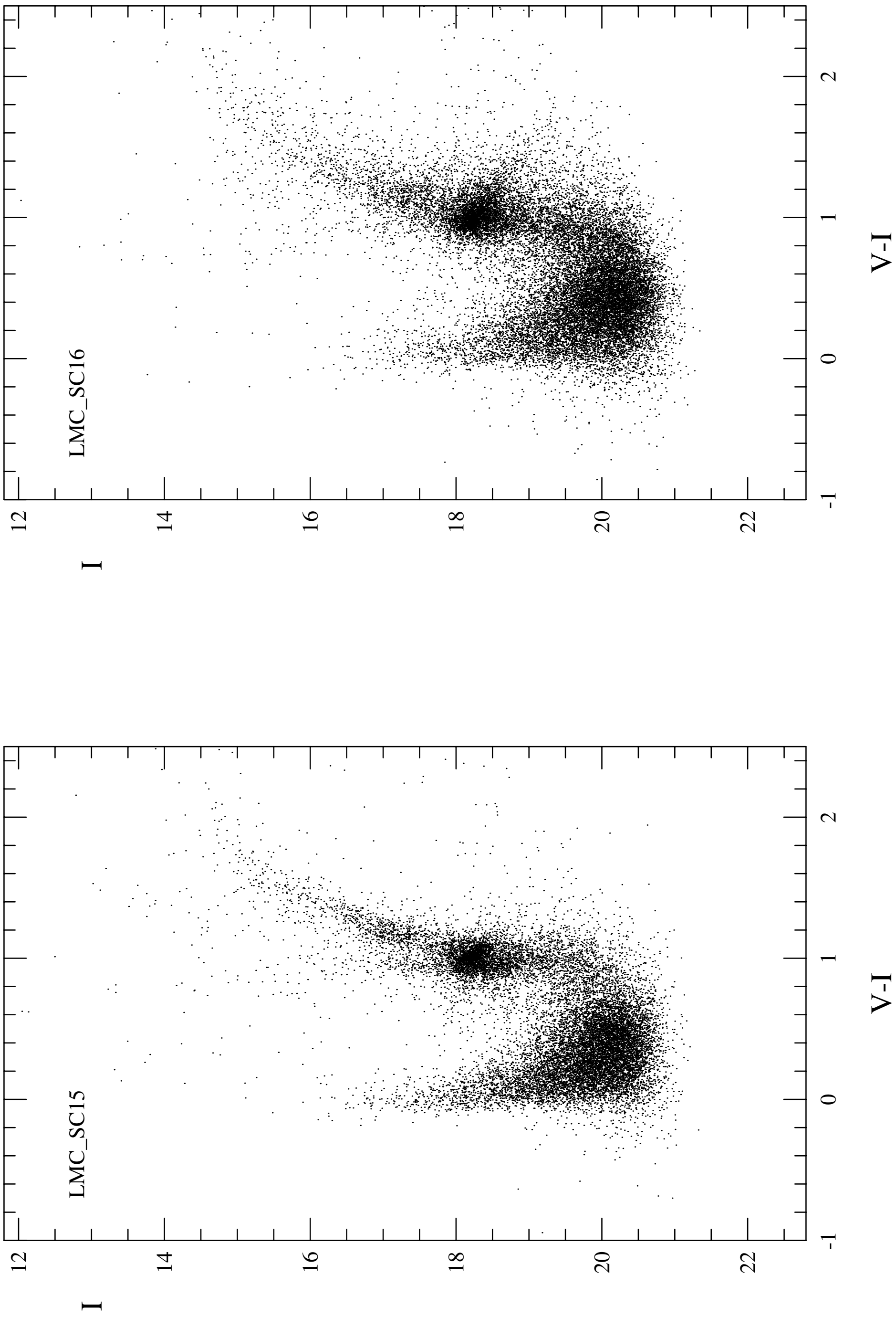

Fig. 14. Color-magnitude diagrams of the fields LMC_SC15 and LMC_SC16.

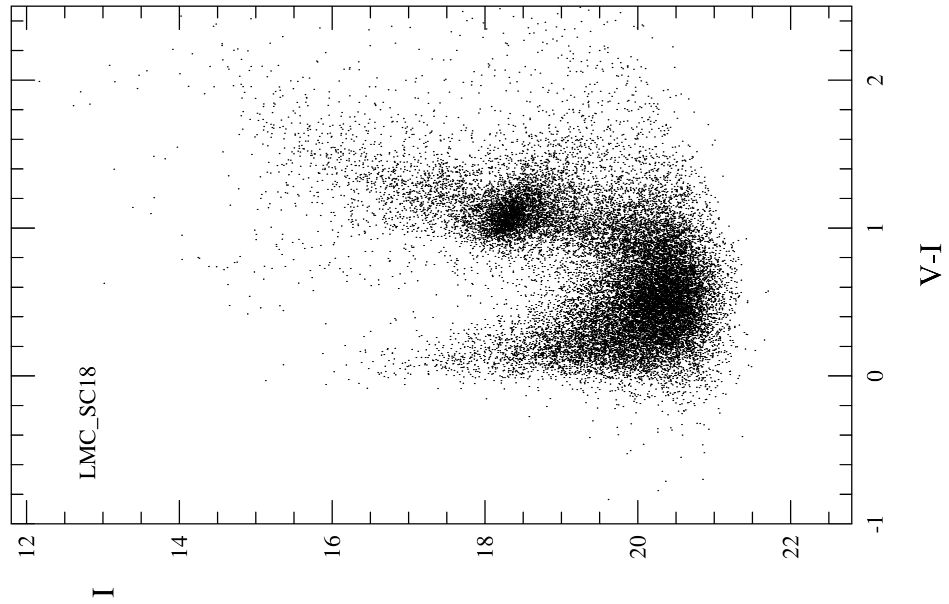

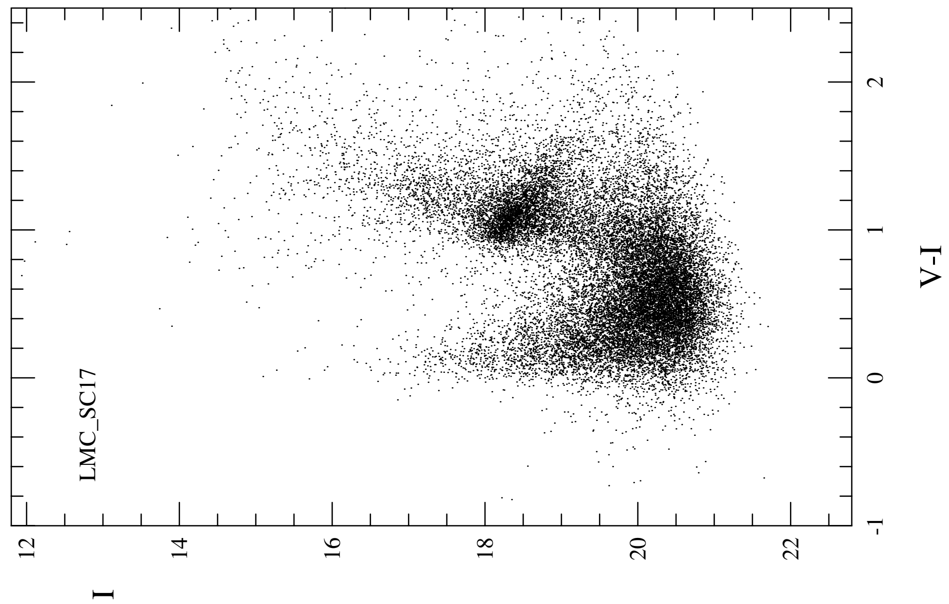

Fig. 15. Color-magnitude diagrams of the fields LMC_SC17 and LMC_SC18.

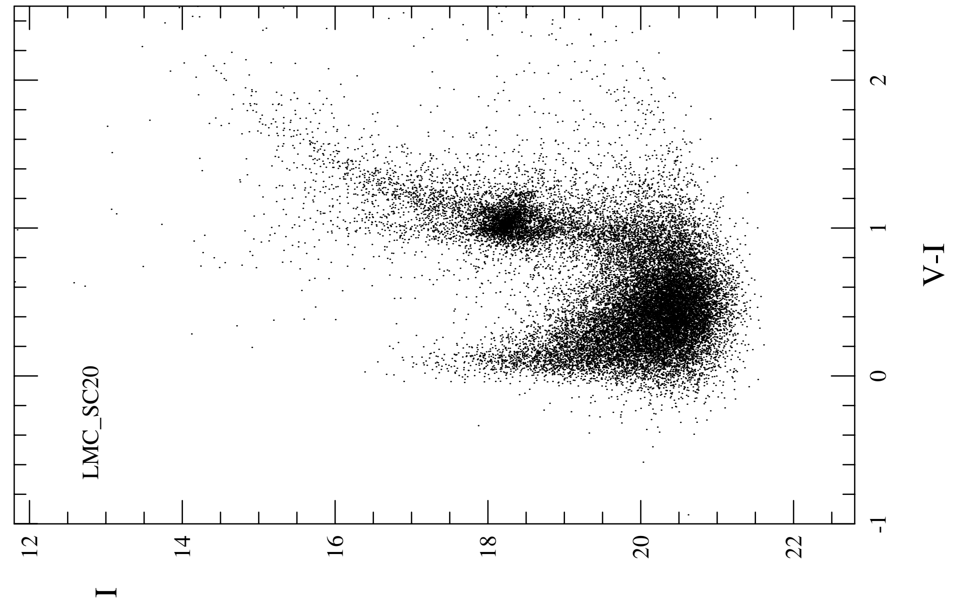

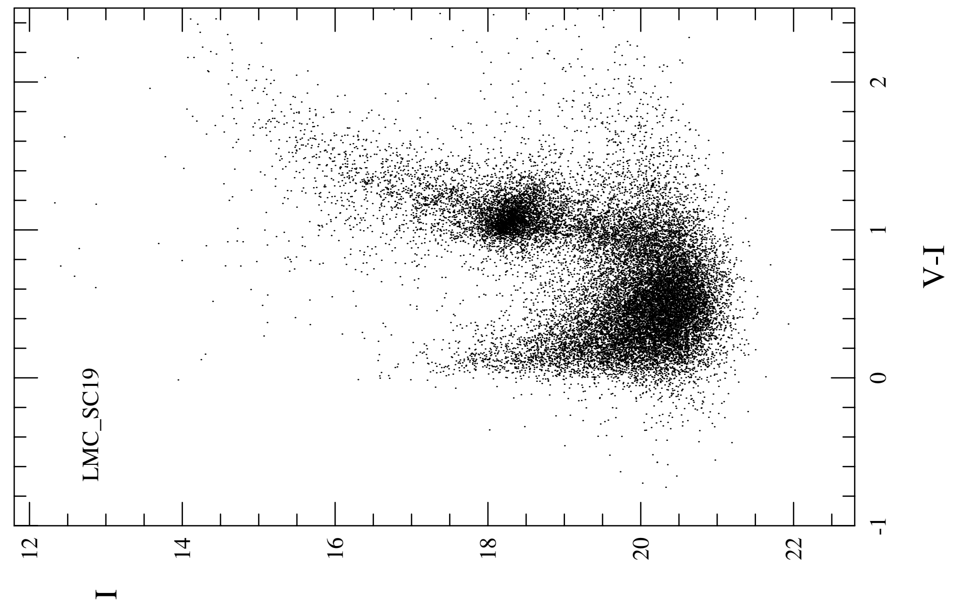

Fig. 16. Color-magnitude diagrams of the fields LMC_SC19 and LMC_SC20.

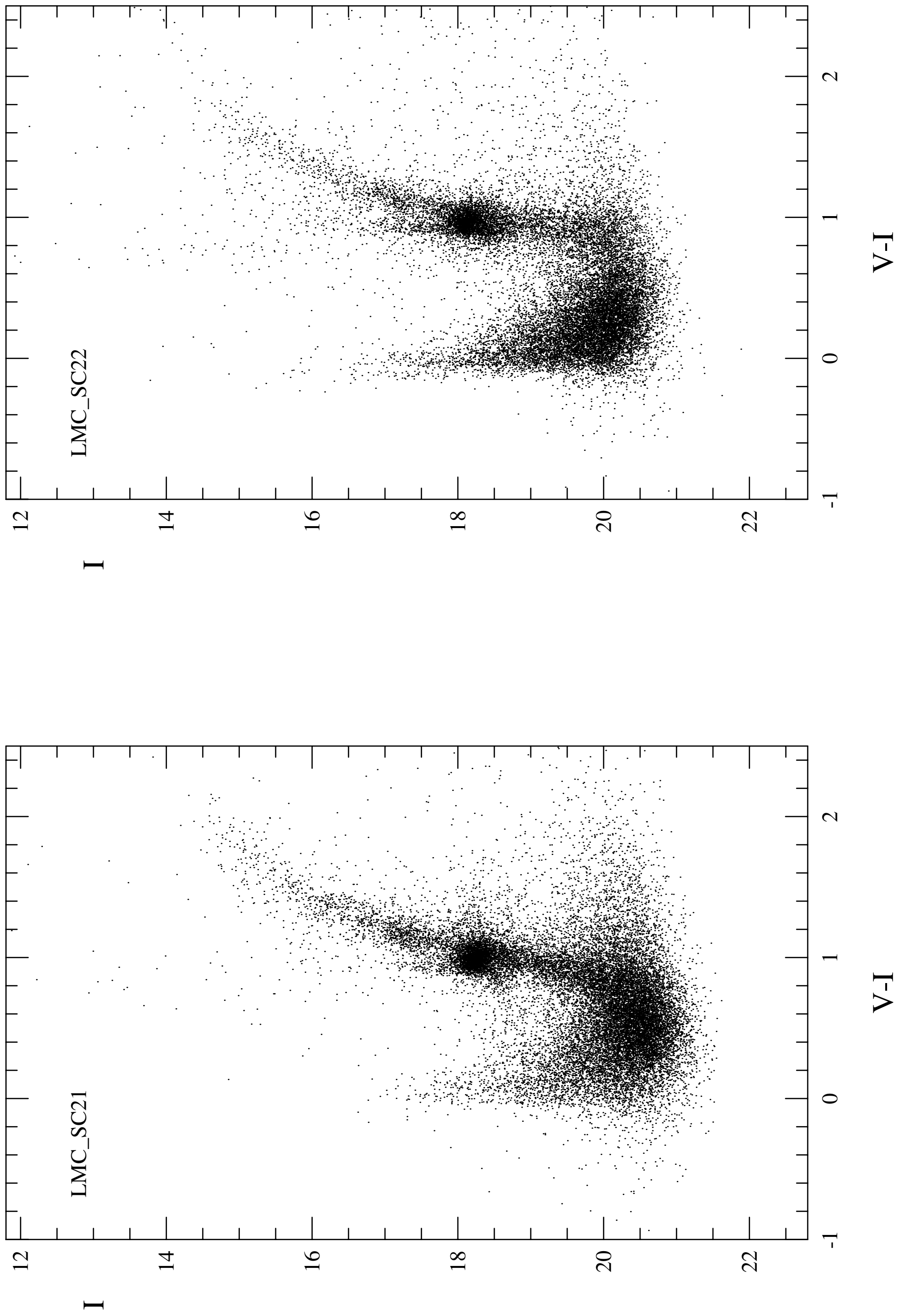

Fig. 17. Color-magnitude diagrams of the fields LMC _ SC21 and LMC _ SC22.

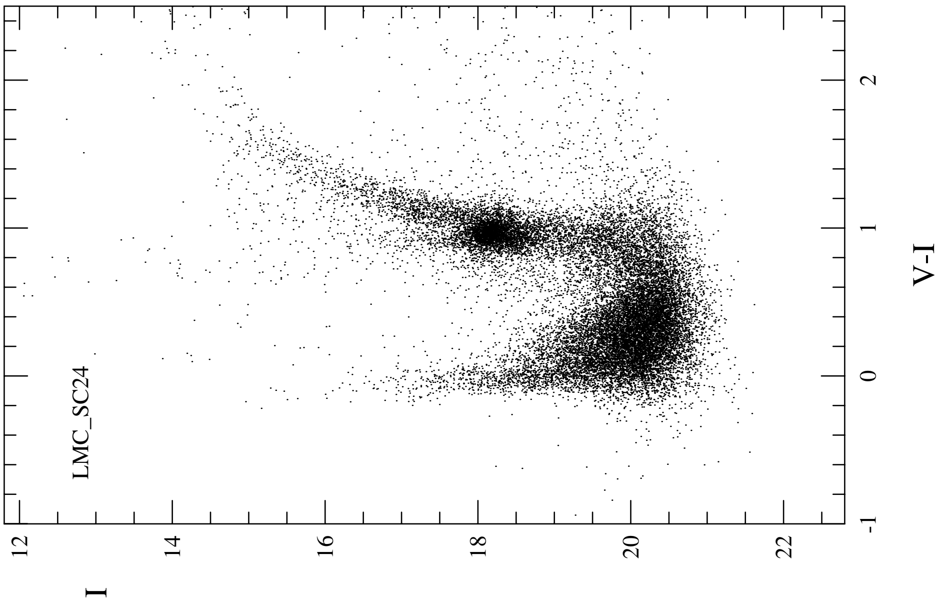

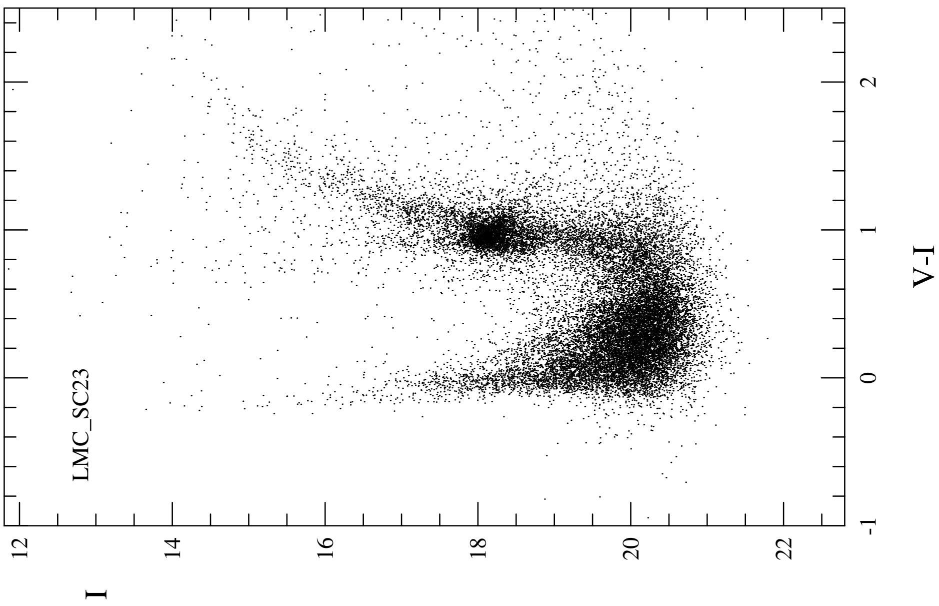

Fig. 18. Color-magnitude diagrams of the fields LMC_SC23 and LMC_SC24.

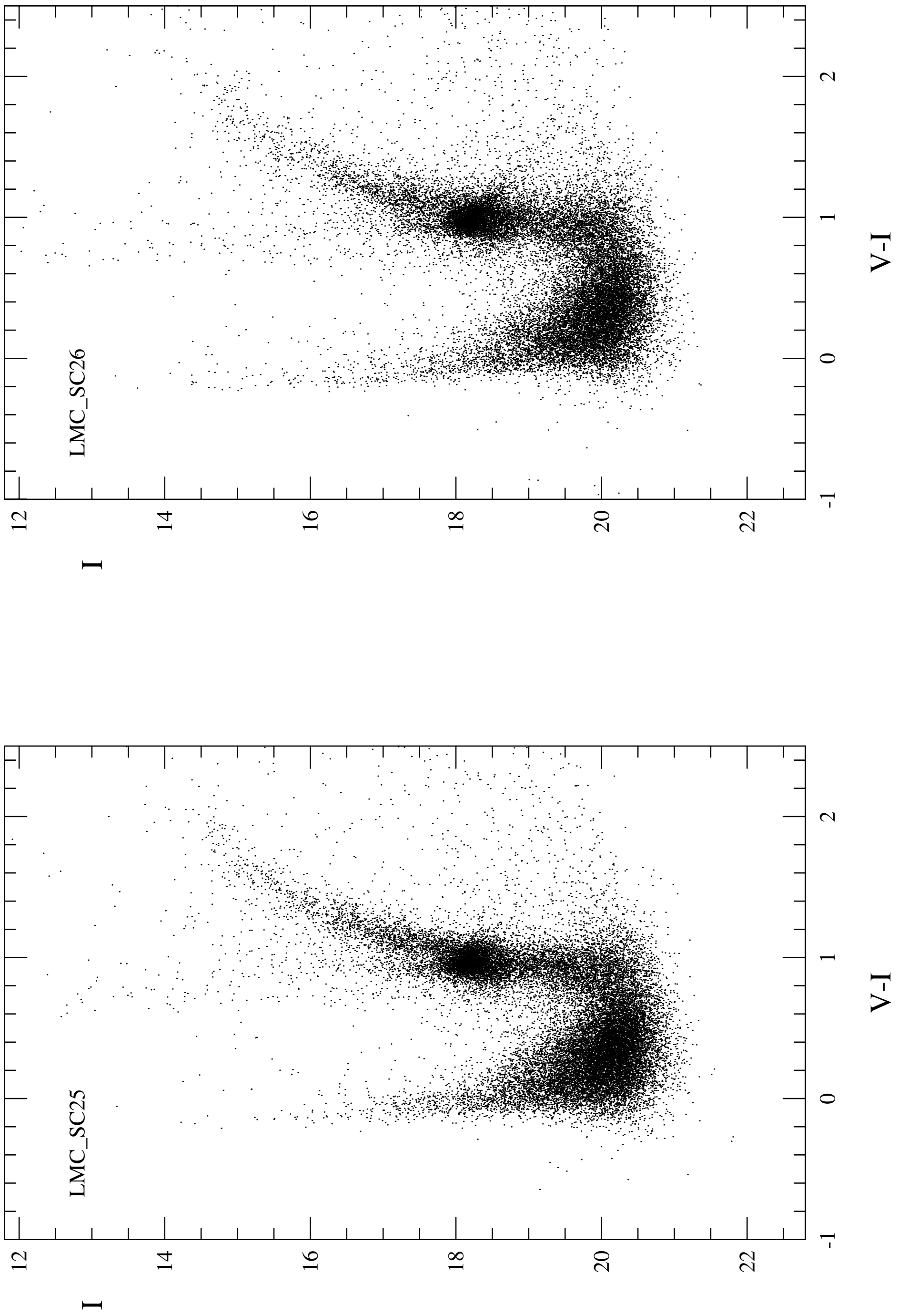

Fig. 19. Color-magnitude diagrams of the fields LMC_SC25 and LMC_SC26.

Table 4

Completeness of the LMC maps

Stars per bin	*B*	Completeness SC_6	SC_12	*V*	Completeness SC_6	SC_12	SC_26	*I*	Completeness SC_6	SC_12	SC_26
2	13.9	99.5	100.0	14.3	99.5	100.0	100.0	13.8	99.5	100.0	100.0
5	14.4	100.0	99.8	14.8	99.8	99.8	100.0	14.3	99.6	99.8	99.8
7	14.9	99.9	100.0	15.3	100.0	100.0	99.9	14.8	99.7	100.0	99.8
10	15.4	100.0	99.6	15.8	99.3	99.8	99.7	15.3	99.2	99.9	99.3
12	15.9	99.5	99.6	16.3	99.3	99.6	99.4	15.8	99.2	99.4	99.7
15	16.4	99.3	99.6	16.8	98.9	99.7	99.6	16.3	98.7	99.5	99.3
17	16.9	98.9	99.8	17.3	97.9	99.5	98.7	16.8	97.6	98.8	99.4
20	17.4	98.9	99.2	17.8	95.6	98.5	98.8	17.3	95.5	98.0	98.3
22	17.9	96.9	99.1	18.3	92.6	97.9	97.9	17.8	92.0	96.9	97.9
25	18.4	95.4	98.5	18.8	86.6	96.0	96.6	18.3	89.0	96.4	96.5
27	18.9	93.1	96.9	19.3	80.0	94.2	93.8	18.8	84.6	94.5	94.4
30	19.4	83.7	93.0	19.8	68.7	90.3	89.3	19.3	74.2	90.8	85.9
32	19.9	69.6	88.1	20.3	52.0	83.8	80.1	19.8	55.0	81.2	45.9
35	20.4	47.8	78.3	20.8	28.5	71.7	59.1	20.3	23.0	51.3	10.3

7. Data Availability

The *BVI* maps of the LMC are available to the astronomical community in the electronic form from the OGLE archive:

http://www.astrouw.edu.pl/˜ogle
ftp://sirius.astrouw.edu.pl/ogle/ogle2/maps/lmc/

or its US mirror

http://bulge.princeton.edu/˜ogle
ftp://bulge.princeton.edu/ogle/ogle2/maps/lmc/

Also *I*-band FITS template images of the OGLE-II fields are included. Total volume of the compressed data is equal to about 0.7 GB. Usage of the data is allowed under the condition of proper acknowledgment to the OGLE project.

We provide these data in the most original form to avoid any additional biases. For instance we do not mask bright stars which often produce many artifacts, but such a masking could potentially remove some interesting information on objects located close to bright stars. We do not remove objects which are located in overlapping areas between the neighboring fields. Cross-identification of these objects can be easily done based on provided equatorial coordinates.

Acknowledgements. We would like to thank Prof. Bohdan Paczyński for many discussions and help at all stages of the OGLE project. We thank Dr. D.S. Graff for information about the systematic error in the early OGLE calibrations. We also thank Mr. A. Olech for carrying out part of the observations of the LMC in the 1997 observing season. The paper was partly supported by the Polish KBN grant 2P03D00814 to A. Udalski and 2P03D00916 to M. Szymański. Partial support for the OGLE project was provided with the NSF grant AST-9820314 to B. Paczyński. We acknowledge usage of The Digitized Sky Survey which was produced at the Space Telescope Science Institute based on photographic data obtained using The UK Schmidt Telescope, operated by the Royal Observatory Edinburgh.

REFERENCES

Alcock, C. *et al.* 2000, *Astron. J.*, **119**, 2194.
Clementini, G., Gratton, R., Bragaglia, A., Carretta, E., and Di Fabrizio, L. 2000, astro-ph/0007471.
Landolt, A.U. 1992, *Astron. J.*, **104**, 372.
Lasserre, T. *et al.* 2000, *Astron. Astrophys.*, **355**, L39.
Schechter, P.L., Saha, K., and Mateo, M. 1993, *P.A.S.P.*, **105**, 1342.
Sebo, K.M., and Wood, P.R. 1995, *Astrophys. J.*, **449**, 164.
Szymański, M., and Udalski, A. 1993, *Acta Astron.*, **43**, 91.
Udalski, A., Kubiak, M., and Szymański, M. 1997, *Acta Astron.*, **47**, 319.
Udalski, A., Szymański, M., Kubiak, M., Pietrzyński, G., Woźniak, P., and Żebruń, K. 1998a, *Acta Astron.*, **48**, 1.
Udalski, A., Szymański, M., Kubiak, M., Pietrzyński, G., Woźniak, P., and Żebruń, K. 1998b, *Acta Astron.*, **48**, 147.
Walker, A.R. 1992, *Astron. J.*, **103**, 1166.
Walker, A.R. 1993, *Astron. J.*, **105**, 527.
Zaritsky, D., Harris, J., and Thompson, I. 1997, *Astron. J.*, **114**, 1002.